Heat Mass Transfer (2009) 45:399–406
DOI 10.1007/s00231-008-0417-1

ORIGINAL

An experimental study of the heat transfer in PS foam insulation

Pen-Chang Tseng · Hsin-Sen Chu

Received: 11 June 2007 / Accepted: 4 June 2008 / Published online: 7 October 2008

Abstract Heat transfer mechanisms in 14 samples of vacuum insulation panels (VIPs) are examined to reveal the influence of porous foam structure on VIP performance. The samples were produced by in-house equipment that was able to vary the foam structure by modulating the process temperature and pressure. Two parameters are proposed to describe the foam structure, namely, the broken cell ratio and the average cell size. Under a specific solid volume fraction, the average cell size shows a linear dependence on the broken cell ratio. Furthermore, the radiation and conduction heat transport data correlate well with these parameters. Radiation heat transfer increases as the broken cell ratio (cell size) increases, but solid conduction decreases as the broken cell ratio (cell size) increases. Consequently, an optimum broken cell ratio (cell size) exists such that the total heat transport is minimum under a specific solid volume fraction. However, the majority of VIP heat transfer is solid conduction. Solid conduction accounts for more than 80% of the total heat transport and is largely affected by the solid volume fraction. A rule of thumb for improving VIP performance is to reduce the solid volume fraction as much as possible to eliminate solid conduction, and maintain the cell size at an optimum value that is dependent on the solid volume fraction.

P.-C. Tseng · H.-S. Chu (✉)
Department of Mechanical Engineering,
National Chiao Tung University,
HsinChu 300, Taiwan, ROC
e-mail: hschu@cc.nctu.edu.tw

P.-C. Tseng
e-mail: PenChangTseng@itri.org.tw

List of symbols

d_c	cell size (μm)
f_s	solid volume fraction (V_s/V_t)
f_{s+g}	volume fraction of combined solid and gas
i_λ	spectral intensity of radiation
k_s	thermal conductivity of solid
k_{s+g}	the equivalent thermal conductivity of combined solid and gas
k_r	the thermal radiation conductivity
k_t	the equivalent total thermal conductivity
m	the weight of the sample
q_{s+g}	the heat flux of combined solid and gas
q_r	radiation heat flux
q_t	total heat flux
T_m	the arithmetic mean of the boundary temperatures (K)
V_b	the broken cell volume
V_s	the volume of solid
V_{s+g}	the volume of combined solid and gas in the unbroken cell
V_t	the apparent volume (total volume)
V_{tb}	the volume of all the cells
V_{ub}	the volume of gas in the unbroken cell

Greek symbols

ρ_f	apparent density or foam density (kg m^{-3})
ρ_s	the density of the solid, 991.96 (kg m^{-3})
ρ_{s+g}	the density of the combined solid and gas in the unbroken cells (kg m^{-3})
σ	Stefan–Boltzmann constant, 5.67×10^{-8} W m^{-2} K^{-4}
σ_e	Rosseland mean extinction coefficient, Eq. (7)
$\sigma_{e\lambda}$	spectral extinction coefficient, τ_λ, spectral transmittance, Eq. (8)
ϕ	broken cell ratio, V_b/V_{tb}, Eq. (9)

1 Introduction

A vacuum insulation panel (VIP), which is constituted of a core porous material enclosed in an evacuated non-permeable package (normally made of metal foil envelopes), features extremely low thermal conductivity and relatively low production cost. These benefits make VIPs suitable for numerous energy conservation applications, such as refrigerator insulation. If the porous cells in the materials are largely open, that is, broken and connected forming a network, evacuating the package to a vacuum could effectively eliminate the gas content and heat transfer by gas convection and conduction. Combining a vacuum with the low conductivity of the porous material, which acts as the VIP's structural support, can greatly reduce overall heat transfer. Commercially available VIPs have currently reached an effective thermal conductivity as low as 4–10 (mW m^{-1} K^{-1}), which is two to six times lower than ordinary foam insulation. However, further reductions in the heat transfer of VIPs require a detailed knowledge of heat transfer mechanisms in the material.

Previous studies have attempted to determine heat transfer in porous foam, including solid conduction [1–5], radiation [6–18] and gaseous conduction [19]. Some of these studies are relevant to VIP applications, and are cited below. Glicksman and Torpey [8] considered a black body strut with an efficiency factor of unity without scattering, and predicted radiation heat transfer in foam using foam density and average cell size. Kamiuto [10] adopted the Dul'nev cubic unit cell model to predict the thermal and radiative properties of open-cellular porous materials for applications in high-temperature heat transfer augmentations. Quenard and Giraud [19] developed an experimental procedure to measure the micro-structural geometrical parameters of a packing of cellular pellets such as EPS foam. A critical value of foam density exists for any given cell size which minimizes effective thermal conductivity. Placido et al. [11] studied the dependence of radiative and conductive properties on the geometrical parameters of closed-cell foam, including mean wall thickness, mean strut diameter, and mean cell diameter. Coquard and Baillis [14] simulated the closed-cell structure of EPS by dodecahedrons and cubes. By solving one-dimensional (1D) steady state coupling equations of radiative and conductive transfer, he found the following parameters pertinent to heat transport, which are listed in order from higher influence to lower influence: foam density, mean cell diameter, inter-bead porosity, and mean bead diameter. Micco and Aldao [15] derived radiative heat transfer rates using a geometrical model and concluded that the geometrical model produced results more similar to experimental values than the Rosseland mean extinction coefficient derivation. Zhao et al. [16, 17] measured the radiative heat transfer of FeCrAlY alloy foam with a high porosity (larger than 95%) and various cell diameters. The extinction coefficients decreased as the cell diameter increased, which has little influence on reflectivity. Both the extinction coefficient and the reflectivity were found to increase as the operation temperature increased.

Most of the studies above assumed all closed-cell or all open-cell structures in their analyses. However, practical applications are far more complicated since the cells in VIPs are not 100% broken, which means that some cells are closed. A cell breaks when forming agents induce enough internal pressure to overcome the cell membrane strength, which depends largely on the viscosity of the material, and therefore on the glass transition temperature (T_g). The material viscosity is relatively high at temperatures above the T_g, but the material hardens immediately when the temperature falls below the T_g. Both features hinder the cell from breaking. It is very difficult to control the material temperature and simultaneously break all the cells inside the material. The positions and number of the unbroken, i.e., closed, cells are hard to control. Nevertheless, cell geometry, including the struts and the residue membranes, plays a key role in both solid conduction and radiative heat transfer in VIPs. Further enhancement of VIP performance requires determining the influence of cell geometry on conduction and radiation, and using this knowledge to improve the manufacturing process. This paper deals with heat transfer in VIPs with partially open cell structures, focusing on VIPs with most of the cells broken. Specifically, more than 90% of the cells are broken and less than 10% of the cells are closed. This high ratio of broken cells is necessary and common in VIPs with satisfactory performance. A total of 14 samples with different cell geometries are produced, and their heat transfer rates are measured and analyzed. The results will be helpful in describing heat transfer in VIPs and serve as a basis for improving VIP performance in the future.

2 Experiments

2.1 Sample fabrication

The samples were prepared by the following procedure. A mixture of polystyrene (97% in weight), carbon black, and calcium stearate were put into a batch die of 400 mm diameter and subjected to a 40-ton press. Foaming was performed by introducing CO_2 and R-134a into the die to form a supercritical fluid after mixing with the molten polystyrene. The high pressure gas in the die was released after 6 h, forming a plain board measuring 250 mm long × 250 mm wide × 6–26 mm thick. After about an hour of heating, the board was enclosed by a metal foil

envelope, which was sealed after the enclosed air was evacuated to 10^{-4} torr. Experiments were designed to vary the cell geometry of the samples by modulating die temperature and gas pressure. Die temperature is controlled by heaters and is maintained at a fixed temperature with a stability of 0.5°C throughout the foaming process. Figure 1 shows the dual pressure control system which was able to separately control the pressure and the amount of CO_2 and R-134a. During the forming process, the gas pressure normally ranged between 2,500 and 3,300 psi. Figure 2 shows a SEM picture of the material sample. The structure typically consists of struts, cell membranes, broken cells, and unbroken cells. A total of 14 samples were produced for analysis in this study, all with partially open cell structures and broken cell ratios (see the definition below) ranging from 90 to 98%.

2.2 Measurements and data reduction

The heat flux (q_t) in VIPs can be divided into the transfer by conduction of solid and gas (q_{s+g}), and by radiation (q_r),

$$q_t = (q_r + q_{s+g}). \quad (1)$$

The concept of equivalent thermal conductivity applies,

$$k_t = k_r + k_{s+g} \quad (2)$$

where k_t is the equivalent total thermal conductivity, k_r is the fraction of equivalent thermal conductivity induced by thermal radiation, and k_{s+g} is the equivalent thermal conductivity of combined solid and gas. In this study, it is further assumed that $k_s \approx k_{s+g}$ since the contribution by gas conduction is relatively small in the samples with broken cell ratio higher than 90%. Note that the heating before sealing and evacuating also helped to eliminate the gases enclosed in closed cells. The equivalent total thermal conductivity was measured by a commercial thermal conductivity meter (EKO HC-072), which was designed in accordance with industrial standards JIS A 1412 and

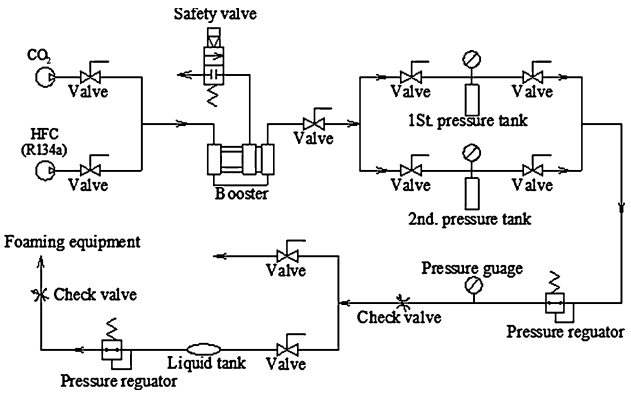

Fig. 1 The dual pressure control system used to modulate the foaming pressure

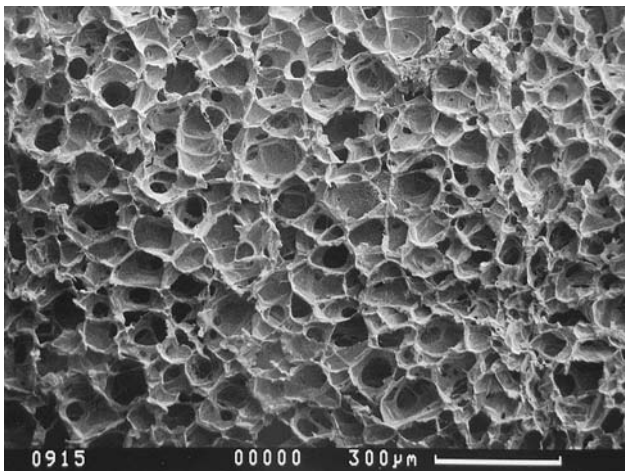

Fig. 2 The SEM picture of sample L4

ASTM 518. The device consists of a hot and a cold plate, thin-film heat-flow meters and a thickness measurement sensor. The temperature of the center of hot and cold plates was measured by the thermocouples. The 250 mm long × 250 mm wide × (6–26) mm thick samples were clapped between the hot and the cold plate with integrated heat flow meters. The following formula is used to calculate the equivalent thermal conductivity.

$$k_t = \frac{EL}{S\Delta T} \quad (3)$$

Where S is the sensitivity of heat-flow meter, ΔT is the temperature difference between the hot and the cold plate, E is the output of the heat-flow meters, and L is the thickness of the sample. The uncertainty was estimated based on the data of Sample L3,

$$\begin{aligned}\Delta k &= \left[\left(\frac{k_t}{q_t}\right)^2 \delta q_t^2 + \left(\frac{k_t}{s}\right)^2 \delta s^2 + \left(\frac{k_t}{\Delta T}\right)^2 \delta \Delta T^2\right]^{0.5} \\ &= \left[\left(\frac{6.6}{23.34}\right)^2 (0.02)^2 + \left(\frac{6.6}{0.00646}\right)^2 (0.00005)^2 \right. \\ &\quad \left. + \left(\frac{6.6}{22.8}\right)^2 (0.1)^2\right]^{0.5} = 0.05896 \ (\mathrm{mW\ mK^{-1}}). \end{aligned} \quad (4)$$

Therefore, the equivalent total thermal conductivity uncertainty can be calculated by, $(\Delta k/k_t) = (0.05896/6.6) = 0.0089$. That is, the uncertainty of measuring specimen total thermal conductivity can be controlled to within 0.89%, as estimated by the method of Wu et al. [13]. The contribution to the equivalent thermal conductivity by radiation is evaluated by the following method. The solid volume fractions of the samples are normally less than 0.06. For the solid phase, over 97% material is polystyrene, which has a refractive index of 1.55. Therefore, if one estimates the refractive index of the foam by weighing the

ratio of solid to void volume, the result would be around 1.03, which is very close to the refractive index of air and vacuum and is neglected in the calculation. The dimensionless optical thickness of a PS sample is evaluated by multiplying its geometrical thickness by its mean extinction coefficient [18]. To be considered optically thick, the value has to be far greater than 1. All the samples in this study obtained the minimum optical thickness of 45. It is therefore satisfactory to assume all samples are optically thick and use the Rosseland mean extinction coefficient, σ_e, by which the radiation heat flux of an absorbing, emitting, and isotropically scattering medium can be written as [20],

$$q_r = -k_r \nabla T = -\frac{16\sigma T_m^3}{3\sigma_e}\nabla T \tag{5}$$

where the equivalent thermal conductivity is defined as

$$k_r = \frac{16\sigma T_m^3}{3\sigma_e} \tag{6}$$

where T_m is the arithmetic mean of the boundary temperatures and σ is the Stefan–Boltzmann constant. The Rosseland mean extinction coefficient, σ_e, is defined as [20]

$$\frac{1}{\sigma_e} = \int_0^\infty \frac{1}{\sigma_{e\lambda}}\frac{\partial e_{\lambda b}}{\partial e}d\lambda. \tag{7}$$

The radiative heat transfer is 1D for a homogeneous planar system, in which the spectral intensity of radiation is governed by the equation of transfer. For the case of a cold homogeneous medium, the emission terms and in-scattering terms are negligible under the influence of a relatively strong but unidirectional beam of radiant energy, and the solution is given by Beer's law. The transmittance is defined as

$$\tau_\lambda = \exp(-\sigma_{e\lambda} s) \tag{8}$$

where $\sigma_{e\lambda} = (\sigma_{\alpha\lambda} + \sigma_{s\lambda})$ is the spectral extinction coefficient.

The spectrum transmittances of the samples were measured by a Perkin Spectrum 2000 Fourier Transform Infrared Spectrometer. For the measurement, a thinly sliced foam specimen was subjected to normal incident irradiation in the wavelength range of 2.5–25 μm. The specimen was first put into an oven to remove its moisture and volatile organic gas contents. With the measured transmittance, the spectral extinction coefficient is calculated by Eq. (8). The term σ_e is then calculated by substituting $\sigma_{e\lambda}$ into Eq. (7) and k_r is subsequently obtained by Eq. (6). With the knowledge of k_r and k_t, k_{s+g} can be inferred from Eq. (2). Note that k_r and k_{s+g} reveal the contribution by radiation and combined solid and gas, respectively. To further distinguish the contribution by solid and by gas, this study introduces a broken cell ratio, ϕ, representing the ratio of broken cell volume to the total cell volume

$$\phi = \frac{V_b}{V_{tb}} = \frac{V_t - \frac{m}{\rho_{s+g}}}{V_t - \frac{m}{\rho_s}} = \frac{\frac{m}{\rho_f} - \frac{m}{\rho_{s+g}}}{\frac{m}{\rho_f} - \frac{m}{\rho_s}} = \frac{\rho_s}{\rho_{s+g}}\frac{(\rho_{s+g} - \rho_f)}{(\rho_s - \rho_f)} \tag{9}$$

where m is the mass of the sample, V_t is the apparent volume (total volume), V_s is the volume of solid, V_{s+g} is the volume of combined solid and gas in the unbroken cell, V_{ub} is the volume of gas in the unbroken cell, V_b is the vacuum volume inside the VIP (which actually contains air in extremely low pressure) or the broken cell volume, and V_{tb} is the volume of all the cells. The apparent density, or foam density, $\rho_f = m/V_t$, was measured using the ASTM D-1622 method. The value $\rho_{s+g} = m/V_{s+g} = m/(V_{ub} + V_s)$ is the density of the combined solid and gas in the unbroken cells. Note that this approach discards the mass of extremely low-pressure gas in the vacuum. Subtracting the broken cell volume from the total volume produces V_{s+g}. The former was measured by an AccuPyc 1330 Pycnometer with an accuracy of 0.03%. The term ρ_s is the density of the solid, taken as the density of the raw polystyrene, which is 991.96 (kg m^{-3}).

The solid volume fraction, f_s, is the ratio of solid volume to the total volume and is readily obtained by dividing the foam density of the sample by the polystyrene density

$$f_s = \frac{V_s}{V_t} = 1 - \frac{(1 - f_{s+g})}{\phi}. \tag{10}$$

The average cell size of each sample was calculated by a method in accordance with ASTM standard D 3576-77, using a SEM picture of the sample.

3 Results and discussions

Table 1 summarizes the measurement results of the 14 samples. The samples fall into two distinct groups with different solid volume fraction. The first group has a lower solid volume fraction (referred to as LSFG) and includes L1–L6 with $0.0413 < f_s < 0.0494$. The second group has a higher solid volume fraction (referred to as HSFG) and includes H1–H8 with $0.0615 < f_s < 0.0706$. The variation of solid volume fraction exerts a profound influence on VIP heat transfer, as explained later. Figures 3 and 4 show examples of spectral transmittance and spectral extinction coefficient, respectively. Note that this spectrum does not reveal CO_2 absorption, which could occur at 2.7, 4.3, 9.4, 10.4, and 15 μm, or H_2O absorption, which could occur at 2.7 and 6.3 μm. This indicates that the amount of CO_2 and H_2O trapped in the unbroken cells is insignificant in terms of influencing radiation heat transfer. This is reasonable

since most of the cells in the samples are broken and evacuated.

Figure 5 plots the broken cell ratio versus the cell size of the 14 samples. The data visibly falls into two groups based on the solid volume fraction. The HSFG cell sizes are typically larger than LSFG cell sizes. Both groups show an almost linear dependence of cell size on open cell ratio. The trend in Fig. 5 can be explained by the fact that a higher solid volume enables the cells to expand further before they are broken, and therefore they have a larger cell size after foaming. On the other hand, to obtain a higher broken cell ratio, some of the unbroken cells must be expanded further until they are broken. Consequently, this also increases the average cell size.

Figures 6 and 7 plots the Rosseland mean extinction coefficient data against variations in cell size and broken cell ratio, respectively. All the extinction coefficient data falls into a single straight line when plotted against the broken cell ratio, as Fig. 7 shows. This indicates that the broken cell ratio is the dominant factor in determining the extinction coefficient. The VIP extinction coefficient consists of two parts, the absorption part, σ_α, and the scattering part, σ_s, that is, $\sigma_e = \sigma_\alpha + \sigma_s$. The former represents the absorption effect of solid material and depends largely on the solid volume fraction. The latter is affected by the geometry of the porous foam structure, which is characterized by the average cell size and the broken cell ratio. For the 14 samples investigated in this study, the solid volume fraction plays a minor role in determining the extinction coefficient, as Fig. 7 indicates. The group with a higher solid volume fraction exhibits only a slight increase in extinction coefficient compared with the lower solid volume fraction group, although the average solid volume

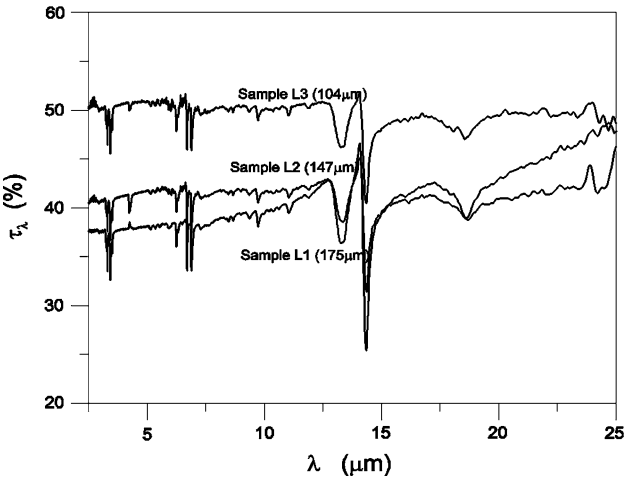

Fig. 3 The transmittance spectrums of several typical samples

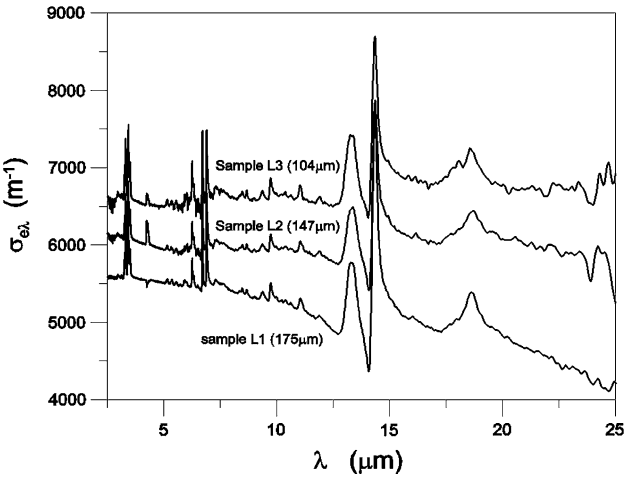

Fig. 4 The spectral extinction coefficients of several typical samples

Table 1 The experimental results of the 14 samples

No. of samples	ρ_f (kg m^{-3})	ρ_{f+g} (kg m^{-3})	f_s	ϕ	d_c (μm)	σ_e (m^{-1})	k_r (mW m^{-1} K^{-1})	k_{s+g} (mW m^{-1} K^{-1})	k_t (mW m^{-1} K^{-1})
L1	49	704	0.0494	0.9787	143	5,397	1.336	5.46	6.8
L2	47	623	0.0474	0.9705	138	5,999.2	1.202	5.50	6.7
L3	44	565	0.0444	0.9649	130	6,653.1	1.084	5.52	6.6
L4	43	486	0.0433	0.9528	119	9,645.9	0.749	5.75	6.5
L5	42	388	0.0423	0.9312	100	13,818.1	0.519	6.48	7.0
L6	41	347	0.0413	0.9198	85	21,887.6	0.327	7.37	7.7
H1	70	812	0.0706	0.9832	374	5,231.8	1.368	6.73	8.1
H2	69	782	0.0696	0.9799	369	5,999.2	1.187	6.71	7.9
H3	68	736	0.0686	0.9744	330	6,291.2	1.132	6.67	7.8
H4	65	709	0.0655	0.9720	318	6,750.3	1.059	6.64	7.7
H5	64	692	0.0645	0.9701	305	7,677.3	0.928	6.67	7.6
H6	63	626	0.0635	0.9604	250	10,758.7	0.664	7.24	7.9
H7	62	561	0.0625	0.9488	175	15,149.4	0.472	7.83	8.3
H8	61	450	0.0615	0.9211	110	20,886.1	0.341	8.66	9.0

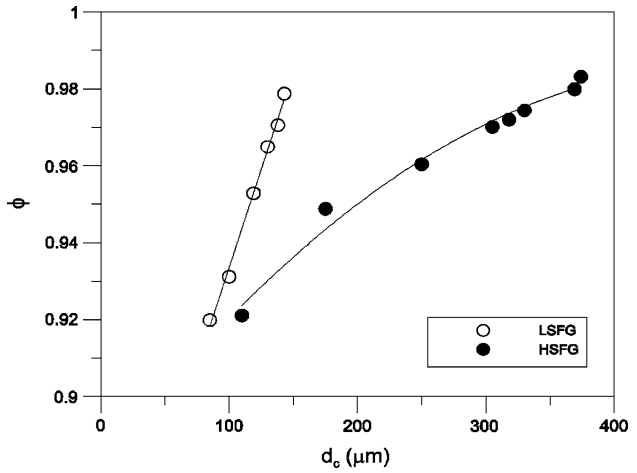

Fig. 5 The relation between average cell size and broken cell ratio, under two different solid volume fractions

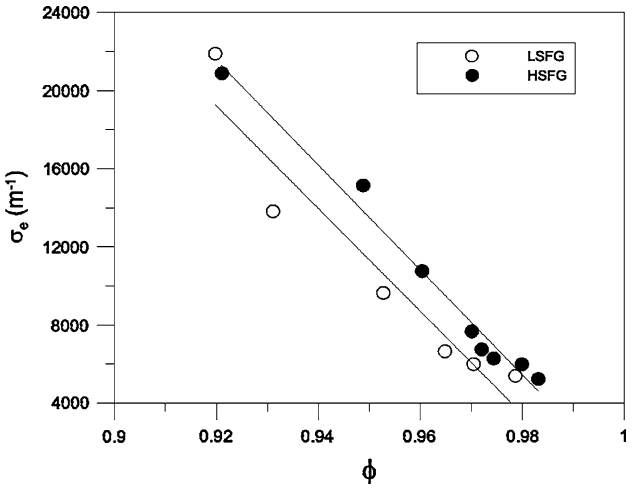

Fig. 7 The effects of broken cell ratio on extinction coefficient, under two different solid volume fractions

fractions of the two groups differ by more than 44% (0.045–0.065). This can be explained by the fact that the solid volume fraction of the samples is so small that the extinction is dominated by scattering and the contribution of absorption is insignificant. The apparent dependence of extinction coefficient on cell size, as Fig. 6 shows, could be interpreted as the dependence on broken cell ratio, since cell size and broken cell ratio are well correlated under a specific volume fraction, as Fig. 5 indicates.

Figure 8 shows the equivalent thermal conductivities of the lower solid volume group, including the total thermal conductivity, k_t, the thermal conductivity by solid conduction, k_s, and the equivalent thermal conductivity by radiation, k_r. Figure 8 shows that as the cell size decreases, which creates more conduction transport routes in the solid material, solid conduction increases. On the other hand, radiation decreases as the cell size decreases. Note that the decrease in radiation (increase in extinction coefficient) is attributable to the change in broken cell ratio, as explained earlier. Consequently, there is a best cell size (best broken cell ratio), which produces the lowest total thermal conductivity after combining k_s and k_r. In Fig. 8, the lowest total thermal conductivity is around 6.5 (mW m^{-1} K^{-1}), which occurs at a broken cell ratio of approximately 0.95 and corresponds to a cell size of about 120 μm. Figure 9 shows the thermal conductivities of the higher solid volume fraction group, with a trend similar to that in Fig. 8. The best broken cell ratio falls at around 0.97, corresponding to a cell size of 300 μm, and results in the lowest total thermal conductivity of 7.6 (mW m^{-1} K^{-1}). Similar dependence of total thermal conductivity on cell size is found in the simulation work by Placido et al. [12], who assumed constant gas contribution in fully closed cell

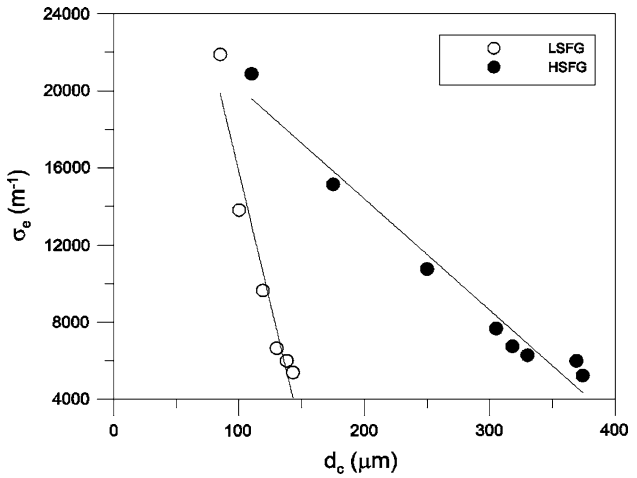

Fig. 6 The effects of average cell size on extinction coefficient, under two different solid volume fractions

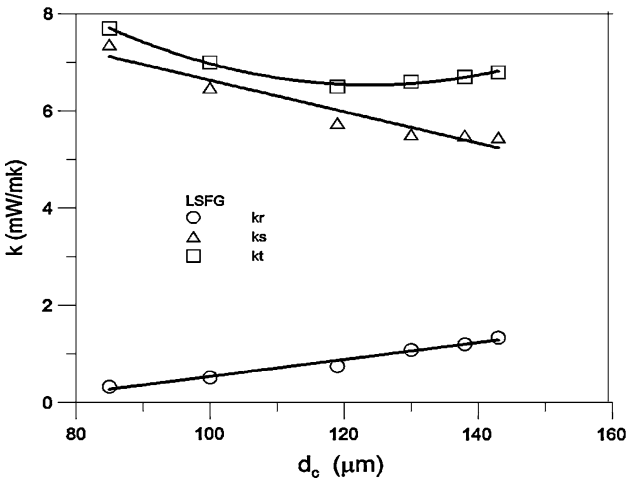

Fig. 8 The influences of average cell size on the LSFG equivalent thermal conductivities

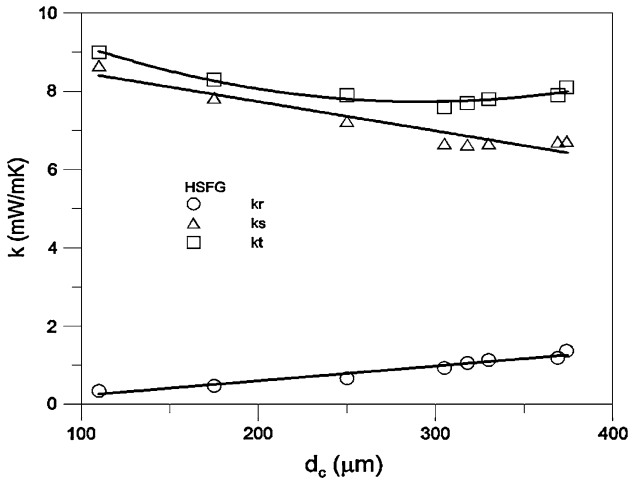

Fig. 9 The influences of average cell size on the HSFG equivalent thermal conductivities

structures and concluded a best cell size of around 100 μm. However, they also concluded that the minimum total conductivity corresponds to the minimum radiative conductivity in fully closed cell structures [11], in contrast to the results of partially open cell structures in Figs. 8 and 9.

The total thermal conductivity of the lower solid volume fraction group (Fig. 8) is generally lower than that of the higher solid volume fraction group (Fig. 9). This difference is caused by a change in solid conduction, which accounts for more than 80% of the heat transfer in the samples (see Figs. 8, 9). The equivalent thermal conductivity of radiation, which is generally responsible for less than 20% of the total heat transfer, shows a relatively weak dependence on the solid volume fraction, which is consistent with earlier observations in Fig. 7. Our earlier study [12] of polyurethane foams revealed the similar proportion of radiative contribution to total heat transfer, namely, 20% of the total heat transfer in vacuum are attributed to radiative transfer.

4 Conclusions

This study analyzes heat transfer in practical VIPs, i.e., VIPs with a broken cell ratio higher than 90%. The structure of these non-black-body VIP foams consists of struts, closed cells, and open cell residue membranes. Two parameters, namely, the broken cell ratio and the average cell size, are proposed to characterize the cell structure. The experimental samples are further grouped based on their solid volume fraction to reveal the influence of the solid material on heat transfer. Some conclusions derived from the experimental findings are summarized below.

1. Radiation heat transfer, as manifested by the mean extinction coefficient, is influenced predominantly by the broken cell ratio. The effects of cell size and solid volume fraction upon radiation are relatively insignificant in the samples investigated in this study.
2. Under a specific solid volume fraction, the best broken cell ratio (best cell size) leads to the lowest total thermal conductivity.
3. Solid volume could affect the absorption coefficient in radiation transfer, but the effects are not obvious because the solid volume fraction is extremely low in this study, and the extinction coefficient is dominated by scattering. However, the solid volume fraction has a crucial effect on solid conduction, which is the dominant heat transfer mechanism in VIP.

A rule of thumb to improve VIP performance can be derived from the findings in this study. Firstly, the solid volume fraction must be kept low to diminish the solid conduction. Secondly, the cell size and broken cell ratio must be carefully controlled to an optimum value to produce the lowest total thermal conductivity. A high broken cell ratio may cause high radiation transfer, and does not necessarily imply low total thermal conductivity. Experimental results of this study suggest a best cell size in the range of 100–300 μm for practical VIP with a high broken cell ratio.

References

1. Chu HS, Stretton AJ, Tien CL (1988) Radiative heat transfer in ultra-fine powder insulations. Int J Heat Mass Transf 31(8):1627–1634
2. Tseng CJ, Yamaguchit M, Ohmorit T (1997) Thermal conductivity of polyurethane foams from room temperature to 20 K. Cryogenics 37(6):305–312
3. Druma AM, Alam MK, Druma C (2004) Analysis of thermal conduction in carbon foams. Int J Thermal Sci 43:689–695
4. Giaretto V, Miraldi E, Ruscica G (1995/1996) Simultaneous estimations of radiative and conductive properties in lightweight insulating materials. High Temp High Press 27/28:191–204
5. Kuhn J, Ebert HP, Arduini-Schuster MC, Buttner D, Fricke J (1992) Thermal transport in polystyrene and polyurethane foam insulations. Int J Heat Mass Transf 35(7):1795–1801
6. Doermann D, Sacadura JF (1996) Heat transfer in open cell foam insulation. ASME J Heat Transf 118:88–93
7. Baillis D, Arduini-Schuster M, Sacadura JF (2002) Identification of spectral radiative properties of polyurethane foam from hemispherical and bi-directional transmittance and reflectance measurements. J Quant Spectrosc Radiat Transf 73:297–306
8. Glicksman LR, Torpey MR (1987) The influence of cell size and foam density on the thermal conductivity of foam insulation. Polyurethanes World Congress, Aachen, Germany. 29 September–2 October, pp 80–84
9. Glicksman LR, Marge AL, Moreno JD (1992) Radiation heat transfer in cellular foam insulation. ASME Paper HTD-203, Developments in Radiative Heat Transfer, pp 45–53
10. Kamiuto K (1997) Study of Dul'nev's model for the thermal and radiative properties of open-cellular porous materials. JSME Int J Ser B 40(4):577–582

11. Placido E, Arduini-Schuster MC, Kuhn J (2005) Thermal properties predictive model for insulating foams. Infrared Phys Technol 46:219–231
12. Wu JW, Sung WF, Chu HS (1999) Thermal conductivity of polyurethane foams. Int J Heat Mass Transf 42:2211–2217
13. Caps R, Heinemann U, Fricke J, Keller K (1997) Thermal conductivity of polymide foams. J Heat Mass Transf 40(2):269–280
14. Coquard R, Baillis D (2006) Modeling of heat transfer in low-density EPS foams. ASME J Heat Transf 128:538–549
15. De Micco C, Aldao CM (2005) Radiation contribution to the thermal conductivity of plastic foams. J Polym Sci [B] 43:190–192
16. Zhao CY, Lu TJ, Hodson HP (2004) Thermal radiation in ultralight metal foams with open cells. Int J Heat Mass Transf 47:2927–2939
17. Zhao CY, Lu TJ, Hodson HP (2004) The temperature dependence of effective thermal conductivity of open-celled steel alloy foams. Mater Sci Eng A 367:123–131
18. Özisik MN (1973) Radiative transfer and interactions with conduction and convection. Wiley, New York
19. Quenard D, Giraud D (1998) Heat transfer in the packing of cellular pellets: microstructure and apparent thermal conductivity. High Temp High Press 30(6):709–715
20. Siegel R, Howell JR (2002) Thermal radiation heat transfer, 4th edn. Taylor & Francis, New York